

#### Contents lists available at ScienceDirect

# Carbon





# Lattice thermal transport in superhard hexagonal diamond and wurtzite boron nitride: A comparative study with cubic diamond and cubic boron nitride



Pranay Chakraborty, Guoping Xiong, Lei Cao\*, Yan Wang\*\*

Department of Mechanical Engineering, University of Nevada, Reno, NV, 89557-0312, USA

#### ARTICLEINFO

Article history:
Received 3 April 2018
Received in revised form
24 May 2018
Accepted 11 June 2018
Available online 14 June 2018

Keywords: Hexagonal diamond Boron nitride Thermal conductivity Phonon First principles

#### ABSTRACT

Hexagonal diamond (h-C) and wurtzite boron nitride (w-BN) are two superhard materials recently identified to be comparable to or even harder than their cubic counterparts, cubic diamond (c-C) and cubic boron nitride (c-BN). To understand the effect of lattice structure on thermal transport in these materials, we conduct first-principles calculations to investigate their harmonic and anharmonic lattice properties. Owing to the strong C-C or B-N bonds, h-C and w-BN are found to have a high lattice thermal conductivity ( $\kappa_L$ ) exceeding the overall thermal conductivity of metals, albeit lower than that of their cubic counterparts. By analyzing the phonon band structure and volume of the 3-phonon scattering phase space, we attribute the lower  $\kappa_L$  of the hexagonal phases to their larger volume of 3-phonon scattering phase space than the cubic ones. Moreover, we reveal that a high pressure of 125 GPa leads to a two-to three-fold increase in the  $\kappa_L$  of these materials, because the pressure enlarges the optical-acoustic phonon bandgap and thus reduces the volume of the 3-phonon scattering phase space. This work uncovers the significant effect of lattice structure and pressure on phonon scattering and transport, which is crucial for the application of superhard materials.

© 2018 Elsevier Ltd. All rights reserved.

#### 1. Introduction

Diamond, of which the lattice can be viewed as a pair of intersecting face-centered cubic lattices, is one of the "supermaterials" that deliver extreme performance across a variety of applications. In particular, it has long been known as one of the hardest and thermally conductive materials on earth. In terms of its thermal performance, theoretical and experimental studies [1–4] have been conducted to investigate thermal transport in both naturally occurring and isotopically pure diamond, revealing that it possesses one of the highest thermal conductivities ( $\kappa$ ) reported so far [5]. The ultrahigh  $\kappa$  of diamond primarily stems from its strong sp<sup>3</sup> C-C bonds and the light carbon atoms, which lead to high phonon group velocities that are higher than most materials in nature. Graphene, another allotrope of carbon with a hexagonal lattice, also has very high  $\kappa$  in the in-plane direction owing to the strong sp<sup>2</sup> C-C bonds and restricted phase space for anharmonic phonon

scattering [5–7]. Owing to their outstanding performance in dissipating heat, there is an increasing interest in applying diamond, graphite, and graphene in thermal management applications [5,7,8]. Diamond, as an excellent electrical insulator, is even preferred when electrical insulation is required.

Similar to those allotropes of carbon, various structures of boron nitride have also been found to possess high  $\kappa$ , though lower than that of diamond and graphene. For example, the room-temperature  $\kappa$  in the basal plane of a bulk sample of pyrolytic hexagonal boron nitride (h-BN) was measured to be up to 390 W/m-K [9]. In 2013, Jo et al. measured the  $\kappa$  of an 11-layer h-BN using a thermal bridge approach and found a value of approximately 360 W/m-K at room temperature, comparable to its bulk-limit value [10]. Later, Zhou et al. obtained room-temperature  $\kappa$ 's between 227 W/m-K and 280 W/m-K for a 9-layer h-BN using the confocal micro-Raman method [11]. Another allotrope of BN, cubic boron nitride (c-BN), was also found to have a high  $\kappa$  of 768 W/m-K from an early experiment [12] or 940 W/m-K from a recent first-principles study [13].

Recently, hexagonal diamond (h-C), a much less understood allotrope of carbon also referred to as lonsdaleite, was found to be

<sup>\*</sup> Corresponding author.

<sup>\*\*</sup> Corresponding author.
E-mail addresses: leicao@unr.edu (L. Cao), yanwang@unr.edu (Y. Wang).

even harder than its cubic counterpart [14]. With a similar structure as h-C, wurtzite boron nitride (w-BN) was also predicted to be ultrahard [14]. As shown in Fig. 1, h-C and w-BN have the same hexagonal lattice structure, which renders it more difficult for lattice planes to glide than their cubic counterparts, c-C and c-BN. Consequently, the hardness of h-C and w-BN are even superior than that of cubic diamond (c-C) and c-BN. Nonetheless, the thermal properties of h-C, c-BN, and w-BN are not well understood yet, inspiring us to investigate their  $\kappa$  and understand how their atomic structures dictate thermal transport properties, which is of both practical and fundamental importance. Moreover, as ultrahard materials are usually used under high-pressure conditions, we will also systematically study how high pressure affects thermal transport in these materials.

### 2. Methodology

The four materials to be studied in this work are insulators with wide electronic bandgap, in which thermal transport is primarily contributed by phonons. Phonons are quanta of lattice vibrations and are usually described with a quantum number,  $\lambda = (\nu, \mathbf{q})$ . In this equation,  $\mathbf{q}$  denotes wave vector and  $\nu$  denotes branch index. The advancement in first-principles based calculation of lattice thermal conductivity  $\kappa_L$  [15–18] has enabled an accurate solution to the linearized phonon Boltzmann transport equation, and, correspondingly, the tensor of  $\kappa_L$  can be calculated as [19].

$$\kappa_L^{\alpha\beta} = \frac{1}{k_B T^2 \Omega N} \sum_{\lambda} f_0(f_0 + 1) (\hbar \omega_{\lambda})^2 \nu_{\lambda}^{\alpha} \mathbf{F}_{\lambda}^{\beta}, \tag{1}$$

in which  $\alpha$  and  $\beta$  are the Cartesian coordinates,  $k_B$  is the Boltzmann constant,  $\Omega$  is the volume of the unit cell, N is the number of discrete  $\mathbf{q}$  points of the  $\Gamma$ -centered  $\mathbf{q}$  grid for sampling the first Brillouin zone (FBZ), f is the Bose-Einstein distribution function,  $\hbar$  is the Planck's constant,  $\omega$  is phonon frequency,  $\nu$  is phonon group velocity, and  $\mathbf{F}$  is usually referred to as "mean free displacement" [19]. The key to obtain  $\kappa_L$  through Eq. (1) is to calculate  $\mathbf{F}_{\lambda}$  using

$$\mathbf{F}_{\lambda} = \tau_{\lambda}^{0}(\mathbf{v}_{\lambda} + \mathbf{\Delta}_{\lambda}),\tag{2}$$

where  $\tau_0$  is the relaxation time, or lifetime, of phonon mode  $\lambda$  and  $\Delta_\lambda$  is a complicated function of **F** [19]. As a result, Eq. (2) has to be solved iteratively. Phonon relaxation time in solids can be limited by various phonon scattering mechanisms, for example, interaction with other phonons, isotopes, impurities, electrons, etc. Under the relaxation time approximation, the 3-phonon anharmonic scattering contribution to the phonon scattering rate  $\gamma_\lambda$ , or the inverse phonon relaxation time, is given by the Fermi's golden rule (FGR) as [20,21].

$$\gamma_{\lambda}^{pp} = \frac{\hbar\pi}{4N} \sum_{\lambda_1 \lambda_2}^{+} 2 \frac{f_1 - f_2}{\omega \omega_1 \omega_2} \left| V_{\lambda \lambda_1 \lambda_2}^{+} \right|^2 \delta(\omega + \omega_1 - \omega_2) 
+ \frac{\hbar\pi}{8N} \sum_{\lambda_1 \lambda_2}^{-} \frac{f_1 + n_f + 1}{\omega \omega_1 \omega_2} \left| V_{\lambda \lambda_1 \lambda_2}^{-} \right|^2 \delta(\omega - \omega_1 - \omega_2).$$
(3)

In the above equation, the first term on the right hand side denotes phonon absorption process, in which two phonons combine into one higher energy phonon; while the second term describes phonon emission process, in which one phonon splits into two lower energy phonons. In addition to the conservation of energy, the lattice or phonon quasi-momentum also needs to be conserved as  $\mathbf{q}_2 = \mathbf{q} \pm \mathbf{q}_1 + \mathbf{Q}$  during the summation over phonon modes in Eq. (3). Here,  $\mathbf{Q}$  is the reciprocal lattice vector with  $\mathbf{Q} = 0$ denoting normal process while  $\mathbf{Q} \neq 0$  denoting Umklapp process. Besides, the Dirac function  $\delta$  is approximated by a Gaussian function following the scheme in Ref. [19], even though the feasibility of Lorentzian function was also demonstrated previously [22]. The 3phonon scattering matrix elements  $V^{\pm}_{\lambda\lambda_1\lambda_2}$  are calculated from the density-functional theory (DFT), of which the details can be found in Refs. [19,21,23,24], while the phonon band structures, or phonon dispersion relations, are calculated through the Fourier transform of the reciprocal-space dynamical matrices obtained from the linear-response theory [25,26]. We only consider three-phonon scattering processes in our calculations, as higher-order phonon scattering processes play an insignificant role in determining the lattice thermal conductivity of the superhard materials studied in this work [27].

In this work, we will consider materials composed of elements (*C*, *B*, or *N*) with natural isotopic distributions as well as isotopically pure materials. The contribution to phonon scattering rates by isotopic disorder can be captured by the well-established model

$$\gamma_{\lambda\lambda_1}^{\text{iso}} = \frac{\pi\omega^2}{2} \sum_{i=1}^{N} g(i) \left| \mathbf{e}_{\lambda}^*(i) \cdot \mathbf{e}_{\lambda_1}(i) \right|^2 \delta(\omega_{\lambda} - \omega_{\lambda_1}), \tag{4}$$

in which i sums over the unit cell. In the above equation, g(i) characterizes the mass disorder among all isotopes as

$$g(i) = \sum_{s} f_s(i) \left[ 1 - \frac{m_s(i)}{\overline{m}(i)} \right]^2, \tag{5}$$

in which  $f_s(i)$  and  $m_s(i)$  denote the frequency of occurrence and the atomic mass of the s'th isotope of atom i, respectively.

We conduct all the DFT calculations using the Quantum ESPRESSO package [25,26]. The Troullier-Martins type normconserving pseudopotentials [28] and the Perdew-Burke-Ernzerhof generalized gradient approximation (PBE-GGA) are used. Prior to calculating the force constants, we conduct structural relaxation

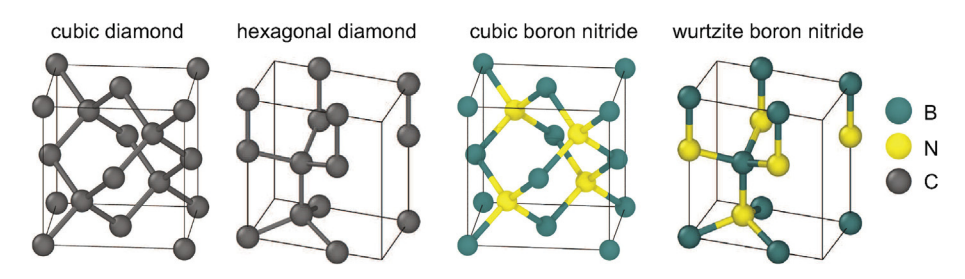


Fig. 1. Lattice structures of the four materials studied in this work. (A colour version of this figure can be viewed online.)

targeting at 0 Pa or 125 GPa to obtain the optimized lattice parameters and atomic positions for the corresponding pressure. A  $16 \times 16 \times 16$  Monkhorst-Pack (MP) grid is used for c-C and c-BN, and a  $16 \times 16 \times 12$  MP grid is used for h-C and w-BN in the structural relaxation and phonon band structure calculations. A plane-wave energy energy cut-off of  $E_{\rm cut}=120$  Ry is used to truncate the plane wave basis set in Quantum ESPRESSO. A  $8 \times 8 \times 8$  **q**-grid is used for phonon band structure calculations for c-C and c-BN, while a  $8 \times 8 \times 6$  grid is used for h-C and w-BN. In the supercell-based 3rd-order force constant (FC) calculations, supercells of  $3 \times 3 \times 3$  primitive unit cells are used for all cases, with atomic interactions considered up to 5th nearest neighbors for c-C and c-BN and to 7th nearest neighbors for h-C and w-BN. A  $3 \times 3 \times 3$  **k**-grid is used in the DFT calculations for 3rd-order FCs.

As the materials studied in this work are pristine, crystalline insulators, the final phonon scattering rates are determined by anharmonic phonon-phonon (p-p) scatterings and isotope scatterings (iso) through the Matthiessen's rule as  $\gamma_{\lambda} = \gamma_{\lambda}^{pp} + \gamma_{\lambda}^{iso}$ , where  $\gamma_{\lambda}^{pp}$  and  $\gamma_{\lambda}^{iso}$  are the anharmonic p-p scattering rates and phonon-isotope scattering rates, respectively. In particular,  $\gamma_{\lambda}^{iso}$  accounts for the effect of mass-difference scattering caused by the coexistence of various isotopes in naturally occurring materials, which can be obtained by integrating the  $\gamma_{\lambda\lambda_1}^{iso}$  in Eq. (4) over all the possible final states  $\lambda_1$ .

#### 3. Results and discussions

Fig. 2 shows the  $\kappa_L$  of the four materials studied in this work, namely, cubic-diamond (c-C), hexagonal-diamond (h-C), cubic boron nitride (c-BN), and wurtzite boron nitride (w-BN), as a function of temperature. Evidently, they all have very high  $\kappa_L$ , which

decreases with temperature owing to the enhanced Umklapp scatterings. Besides, our results for c-C at zero pressure agree with previous experimental data [3,29] and Broido et al.'s first-principles calculations [4] very well, as shown in Fig. 2a, which validates the methodology used in our work. Thermal transport in cubic diamond is already well understood and it is not surprising to see an anisotropic thermal conductivity of hexagonal diamond and wurtzite boron nitride, either. However, it is interesting to see that h-C and w-BN have significantly lower thermal conductivity than their cubic counterparts, c-C and c-BN, respectively, at zero pressure, even though they have the same bonding environment. In particular, as shown in Fig. 2a, the room-temperature  $\kappa_L$  of isotopically pure c-C is 3398 W/m-K, while that of isotopically pure h-C is only 2389 W/m-K in the x-y directions. The  $\kappa_L$  of h-C is even lower in the z direction (2009 W/m-K). Similarly, as shown in Fig. 2c, the room-temperature  $\kappa_L$  of isotopically pure c-BN is 1905 W/m-K, while that of isotopically pure w-BN in the x-y directions and z direction is only 1344 W/m-K and 1155 W/m-K, respectively. A deeper understanding of the mechanism of such difference in  $\kappa_L$  will shed light on how lattice structure and the arrangement of atoms affect thermal transport in materials.

Typically, stiffer bonds, i.e., higher bond energy, would lead to larger phonon group velocity and thus higher  $\kappa_L$ , which partly contributes to the high  $\kappa_L$  of several carbon based allotropes, including c-C, graphene, and carbon nanotube. Therefore, we compare the bulk modulus B of c-C (c-BN) and h-C (w-BN) to check whether a difference in bond energy causes the significant difference between their  $\kappa_L$ 's. Bulk modulus quantifies the compressibility of the material, i.e., its volumetric change in response to the applied hydrostatic pressure. It is one of the material properties commonly used to quantify how hard the material is. Atomistically,

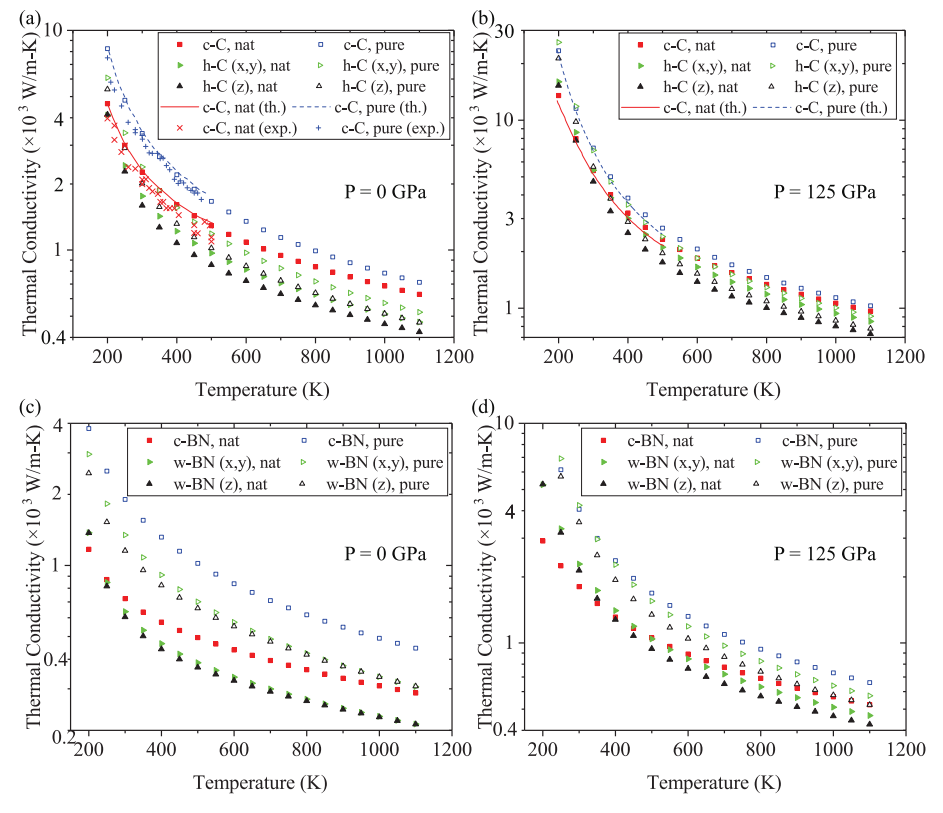


**Fig. 2.** Thermal conductivity as a function of temperature for cubic diamond and hexagonal diamond at 0 GPa (a) and 125 GPa (b), and for cubic boron nitride and wurtzite boron nitride at 0 GPa (c) and 125 GPa (d). In panel (a) and (b), we also compare our calculated values of  $\kappa_L$  with experimental (exp.) data [3,29] and theoretical (th.) data [4]. (A colour version of this figure can be viewed online.)

the stretchability of the chemical bonding, bond type, and bond length dictate the bulk modulus. Here we calculate the *B* of the four superhard materials based on the thermodynamic definition,

$$B = -\frac{dP}{dlnV} = V\frac{d^2E}{dV^2},\tag{6}$$

where P is the pressure, V is the volume, and E is the total energy. We apply pressures ranging from -25 kbar to 25 kbar to compress or stretch the unit cell, which is fully relaxed to energy minimum under the corresponding pressure in Quantum ESPRESSO. Afterward, we fit the total energies and the corresponding volumes of the relaxed unit cells quadratically using the least-mean-square scheme [27], through which we can obtain  $d^2E/dV^2$ . Finally, B can be obtained through Eq. (6).

Table 1 shows the calculated Bs. Obviously, the B of c-C is only 1% different from that of h-C and the B of c-BN is only 2% different from that of w-BN. Moreover, c-C (c-BN) and h-C (w-BN) also share almost the same C-C (B-N) bond length, as shown in Table 1. These findings suggest that c-C (c-BN) has almost the same bonds as h-C (w-BN). Therefore, bond energy difference is not the reason for the difference in the  $\kappa_I$  of c-C (c-BN) and h-C (w-BN).

To confirm the above conclusion, we also conduct equilibrium molecular dynamics simulations using the Tersoff potential [38,39] for both c-C and h-C, and then use the Green-Kubo method [40–42] to calculate  $\kappa_L$ . Specifically, the thermal conductivity tensor is calculated from the heat current autocorrelation function (HCACF) as

$$\kappa_{\alpha\beta} = \frac{V}{k_B T^2} \int_0^{\tau} \left\langle J_{\alpha}(t) J_{\beta}(0) \right\rangle dt, \tag{7}$$

in which V is the volume of the simulation domain, T is temperature,  $k_B$  is the Boltzmann constant, J is the Cartesian components of the heat flux vector  $\mathbf{J}$ , and t is time. The subscripts  $\alpha$  and  $\beta$  are Cartesian coordinates,  $\mathbf{x}$ ,  $\mathbf{y}$ , or  $\mathbf{z}$ .  $\mathbf{J}$  is computed as

$$\mathbf{J}(t) = \frac{1}{V} \left\{ \sum_{i} \mathbf{v}_{i} \varepsilon_{i} + \frac{1}{2} \sum_{i,j,i \neq j} \mathbf{r}_{ij} (\mathbf{F}_{ij} \cdot \mathbf{v}_{i}) + \sum_{i,j,k} \mathbf{r}_{ij} [\mathbf{F}_{j}(ijk) \cdot \mathbf{v}_{j}] \right\},$$
(8)

in which the subscripts i,j, and k are atom indexes,  $\mathbf{v}$  is the atomic velocity,  $\varepsilon$  denotes the energy of the atom,  $\mathbf{r_{ij}}$  is the distance vector between atoms i and j, and  $\mathbf{F}$  is force resulting from the 2-body  $(F_{ij})$  or 3-body  $(F_{ijk})$  interactions between atoms i, j, and k. In our simulation, a  $3.9 \times 3.9 \times 3.9 \,\mathrm{mm}^3\,\mathrm{c-C}$  supercell and a  $3.5 \times 3.5 \times 3.3\,\mathrm{mm}^3\,\mathrm{h-C}$  supercell are simulated in the LAMMPS package [43] with the periodic boundary condition applied to all the three dimensions. The carbon atoms are initialized with random velocities following a Gaussian distribution at 5 K. Then the structure is first relaxed in the NPT ensemble by a Nose'-Hoover thermostat at zero pressure with the temperature increasing from 5 K to 300 K in 400 ps, followed by a NPT relaxation at zero pressure and 300 K for another 1 ns. Finally, the simulation is switched to the NVE ensemble for 10 ns, from which the instantaneous heat fluxes are

calculated and recorded for Green-Kubo calculations. In the foregoing molecular dynamics simulations, a time step size of 1 fs is used to ensure numerical accuracy. For the Green-Kubo calculation, 3 independent simulations for c-C and 9 independent simulations for h-C are conducted, among which carbon atoms are initialized with different velocities at the beginning of the simulation, so that we can extract statistically more accurate  $\kappa_L$  from the integral of the averaged HCACF curves. We find that the  $\kappa_L$  of c-C is 1,866±126 W/ m-K, which agrees well with Fan et al.'s result (1950±40 W/m-K) [44] obtained from Green-Kubo calculations using the same Tersoff potential. Moreover, the  $\kappa_L$  of h-C in the x-y direction is found to be 1,  $200\pm50$  W/m-K and that in the z direction is  $645\pm173$  W/m-K, which are lower than that of c-C. This is also true at other temperatures, as shown in the Supplementary Materials [27]. Obviously, the bond strength of the c-C and h-C in our simulations should be the same, because they are described by the same interatomic potential; hence the notable difference in  $\kappa_L$  should come from other resources.

The primitive unit cell of c-C has two carbon atoms while that of h-C has four. Therefore, h-C has more optical phonon branches than c-C, i.e., h-C has nine while c-C has three. In fact, we can view the added optical branches in h-C as if they are generated by Brillouin zone folding, through which each of the three acoustic phonon branches in c-C is folded and split into one acoustic phonon branch and one optical phonon branch. The folding process can generate a bandgap, which effectively reduces the slope (phonon group velocity) of the dispersion curves. This mechanism has been used to explain the reduced  $\kappa_L$  of superlattices when the size of the unit cell (period thickness) increases [45–47]. To isolate such effect of phonon band structure from that caused by lattice anharmonicity, we calculate the volumetric heat capacity and small-grain-limit thermal conductivity, which are defined as

$$c_{v} = \frac{k_{B}}{(2\pi)^{3}} \int_{FBZ} \left(\frac{\hbar\omega}{k_{B}T}\right)^{2} f_{0}(f_{0}+1) d^{3}\mathbf{q}$$
 (9)

and

$$\kappa_{L,SG}^{\alpha\beta} = \frac{1}{k_B T^2 \Omega N} \sum_{\lambda} f_0(f_0 + 1) (\hbar \omega_{\lambda})^2 \frac{\nu_{\lambda}^{\alpha} \nu_{\lambda}^{\beta}}{|\mathbf{v}_{\lambda}|}, \tag{10}$$

respectively. It is worth emphasizing that the  $c_v$  and  $\kappa_{L,SG}$  calculated in the above way are solely determined by harmonic lattice properties, if we neglect the effect of lattice anharmonicity on phonon dispersion relations. As shown in Fig. 3a, there is no notable difference between the  $c_v$  of c-C and h-C, and similarly for c-BN and w-BN. This is expected because all the structures are closely packed with a C-C bond length of 1.54 Å or B-N bond length of 1.56 Å based on Table 1. According to Fig. 3b, however, the room-temperature  $\kappa_{L,SG}$  of c-C (c-BN) is indeed higher than that of h-C (w-BN). Specifically, the  $\kappa_{L,SG}$  of c-C is 4.37 W/m-K, 7% higher than that (4.09) of h-C. Similarly, the  $\kappa_{L,SG}$  of c-BN is 4.45 W/m-K, 10% higher than that (4.03) of w-BN. Evidently,  $\kappa_{L,SG}$ , or the phonon band structure, can explain part of the observed higher  $\kappa_L$  of c-C (c-BN) than h-C (w-BN), but the majority of the difference should arise from

**Table 1**The bulk modulus and lattice parameters (*a*) of c-C, h-C, c-BN, and w-BN obtained from this work and from literature (lit.).

Material	B (GPa)	B (GPa), lit.	a (Å)	a (Å), lit.
c-C	425.7	442 [30], 445.6 [31]	3.560	3.567 [32]
h-C	431.4	456.0 [31]	2.504	2.52 [33,34]
c-BN	374.3	369±14[35], 401 [36], 375 [36]	3.612	3.615 [37], 3.617 [36]
w-BN	366.1	373 [36]	2.546	2.549 [36]

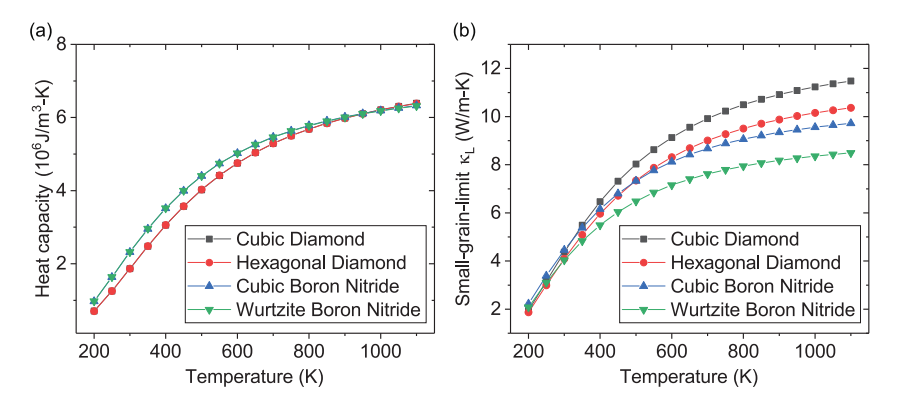


Fig. 3. Heat capacity (a) and small-grain-limit lattice thermal conductivity (b) of the four materials. (A colour version of this figure can be viewed online.)

anharmonic properties.

To test the above hypothesis, we compare the phonon scattering rates of c-C with those of h-C. Fig. 4a and c shows the anharmonic phonon scattering rates for the longitudinal acoustic (LA) phonon modes located at the  $q_x$ - $q_y$  plane of the FBZ of c-C and h-C, respectively. As we can see, the scattering rates of the LA phonons in h-C are significantly higher than those in c-C. In fact, the contribution to the room-temperature  $\kappa_L$  by LA modes in c-C is 1403 W/m-K, while it has a much lower value of 635 W/m-K in h-C. Other than LA modes, we also found similar behaviors for the TA phonon modes in c-C and h-C. Since the harmonic lattice properties, e.g.,  $c_v$  and  $\kappa_{LSG}$ , are not much different between c-C and h-C, we can conclude that the different  $\kappa_L$  of the two materials is mainly caused by the difference in phonon scattering rates. This conclusion also applies to c-BN and w-BN. As shown in Fig. 4b and d, the phonon scattering rates in w-BN are also much higher than those in c-BN.

To explore the fundamental reason for the higher phonon scattering rates in c-C (c-BN) than in h-C (w-BN), we need to revisit Eq. (3), based on which we obtained the anharmonic phonon scattering rates. Obviously, there are two possible mechanisms for the difference in  $\kappa_L$ : (1) the 3rd-order force constants, which directly determines the value of the 3-phonon scattering matrix elements  $V_{\lambda\lambda_1\lambda_2}^{\pm}$  in Eq. (3), are larger in h-C than in c-C; (2) the 3phonon scattering phase space, which quantifies the amount of possible 3-phonon combinations satisfying both momentum and energy conservation, is larger for the acoustic phonon modes (major heat carriers) in h-C than in c-C. The first mechanism is quite unlikely, because our bulk modulus calculation already indicates that the two materials have rather similar bonds. In fact, considering that there are more optical phonon branches in h-C than in c-C, and that the optical-acoustic phonon bandgap is much smaller in h-C, it is reasonable to expect a larger phonon scattering phase space in h-C than in c-C.

Typically, the volume of the scattering phase space P is defined for each  $\mathbf{q}$ -mesh with a finite volume  $\delta V_q$  [19]. To make a fair comparison between different material systems or different calculations, in which there might be a mismatch in the size of  $\mathbf{q}$ -mesh in the FBZ, we define a differential 3-phonon scattering phase space,  $\partial P/\partial V_q$ , as

$$\frac{\partial P}{\partial V_{\mathbf{q}}}(\mathbf{q}) = \frac{N\Omega}{(2\pi)^3} \sum_{\nu'\nu''} \int_{FBZ} \delta \left[ \omega_{\nu}(\mathbf{q}) \right] + \omega_{\nu'} \left( \mathbf{q}' \right) \right] - \omega_{\nu''} \left( \mathbf{q} + \mathbf{q}' - \mathbf{Q} \right) d^3 \mathbf{q}'.$$
(11)

The physical meaning of  $\partial P/\partial V_q$  is the total volume of scattering phase space per unit volume of the **q**-mesh for a specific phonon

mode  $\lambda=(\nu,{\bf q})$ . As shown in Fig. 4e and f, the LA phonons in h-C has a larger  $\partial P/\partial V_q$  than those in c-C. Moreover, we also confirm that this only occurs for absorption processes, in which one LA phonon combines with another phonon into a higher-energy acoustic or optical phonon. Evidently, a smaller optical-acoustic phonon bandgap could facilitate such process, because it becomes easier for the LA phonon to absorb another phonon to become higher-energy optical phonons. Similar conclusion also holds for c-BN and w-BN, which confirms our hypothesis above.

Since physical properties of superhard materials under high pressure are always of great interest, herein we compare lattice thermal transport in these materials at 0 Pa and 125 GPa. By comparing the data in Fig. 2a and b, we can see that a pressure of 125 GPa increases the  $\kappa_L$  of c-C and h-C greatly. Specifically, the room-temperature  $\kappa_L$  of isotopically pure c-C has increased more than two-fold from 3398 W/m-K to 7103 W/m-K, while that of isotropically pure h-C (x-y direction) has increased from 2389 W/ m-K to 6911 W/m-K. Similarly, we can also find a more than twofold increase in  $\kappa_L$  for c-BN and w-BN by comparing the data in Fig. 2c and d. A compressive strain typically increases the phonon group velocity, which can increase the  $\kappa_L$  of materials based on Eq. (1). To investigate whether this is the reason for the increased  $\kappa_L$  in these materials under high pressure, we plot the phonon dispersion relations in Fig. 5. Obviously, the high pressure has increased the frequency of all phonon modes in the materials. In particular, the slopes of all the 3 acoustic branches are increased, which means the group velocities of those acoustic phonon modes have increased. However, the increase is less than 10%, which cannot explain the more than two-fold increase in  $\kappa_L$  displayed in Fig. 2. Therefore, we further compare the phonon scattering rates of the four materials at 0 Pa and 125 GPa. As revealed by Fig. 6a-d, the phonon scattering rates in unstrained materials are obviously higher than those under 125 GPa. Specifically, an approximately two-fold difference between the scattering rates is induced by the applied pressure, which should be the major cause of the more than two-fold difference in  $\kappa_I$ . In fact, we can observe a prominent enlargement in the optical-acoustic bandgap in all the four panels in Fig. 5. An increased phonon bandgap usually makes it more difficult for phonon modes to pair with other modes to satisfy both momentum and energy conservation for 3-phonon scattering processes to occur or, in other words, reduces the volume of 3-phonon scattering phase space. As shown in Fig. 6e and f,  $\partial P/\partial V_q$  of the LA phonons is generally lower in the materials under 125 GPa, which explains our observation of the weakened phonon scatterings and thus enhanced thermal conductivity at high pressure.

Finally, as these materials are usually found in polycrystalline forms or of very small size, it is beneficial to understand how

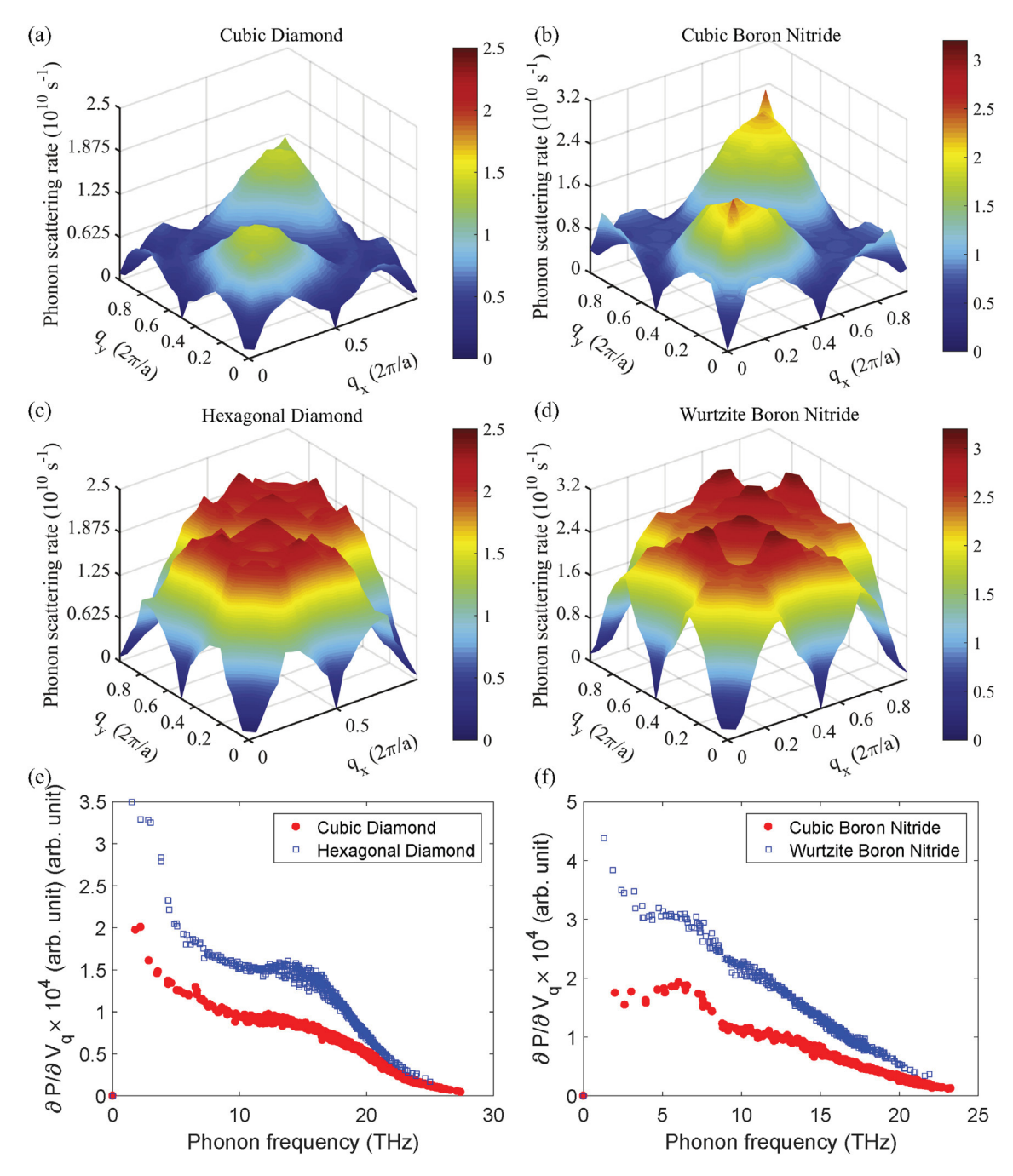


**Fig. 4.** Panels (a)—(d) show the anharmonic phonon scattering rates at 300 K for longitudinal phonon modes on the  $q_x$ – $q_y$  plane of the FBZ of c-C (a), c-BN (b), h-C (c), and w-BN (d). Panels (e) and (f) display the differential volume of the 3-phonon scattering phase space for the four materials. (A colour version of this figure can be viewed online.)

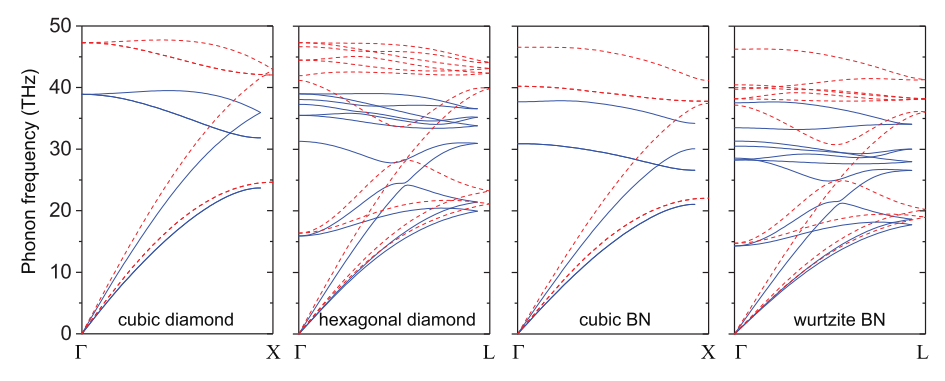
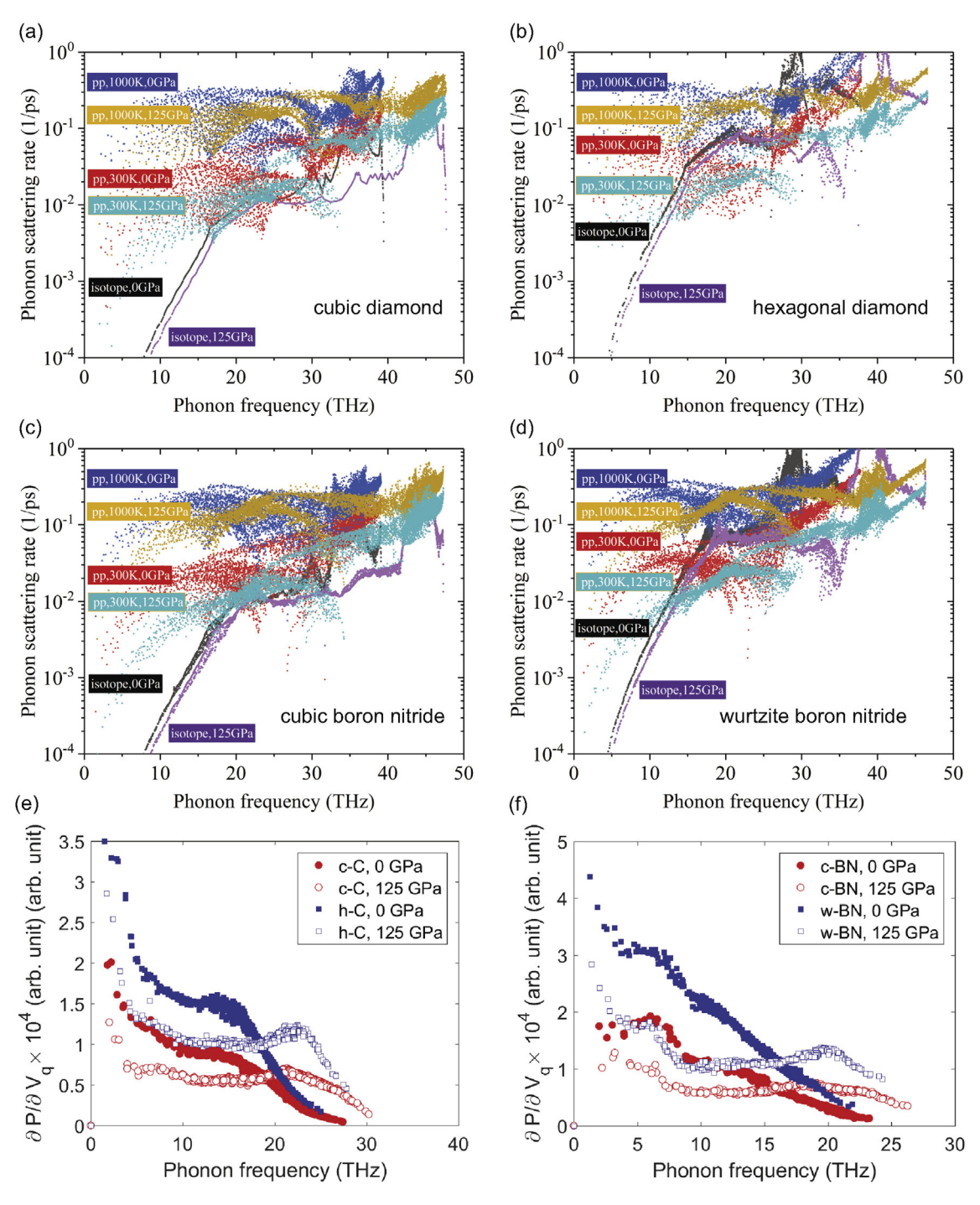


Fig. 5. Phonon dispersion relations for the four materials at 0 Pa (blue solid curves) or 125 GPa (red dashed curves). (A colour version of this figure can be viewed online.)



**Fig. 6.** Spectral phonon scattering rates owing to anharmonic 3-phonon scattering and isotope scattering at 300 K for (a) cubic diamond, (b) cubic boron nitride, (c) hexagonal diamond, and (d) wurtzite boron nitride. (e) and (f) show the differential volume of the 3-phonon scattering phase space for the four materials under 0 GPa and 125 GPa. (A colour version of this figure can be viewed online.)

structure size affects the lattice thermal conductivity. The cumulative lattice thermal conductivities (as a function of the phonon mean-free-path) of the four materials at 0 Pa and 300 K are plotted in Fig. 7, which approximately quantify how  $\kappa_L$  can be truncated by a specific material size. As we can see, lattice thermal transport in these materials is mainly contributed by phonons with a mean-free-path of 0.2–2  $\mu$ m. In other words, grain size or material size in or smaller than this range can reduce the  $\kappa_L$  of these materials significantly.

## 4. Summary

To summarize, we have conducted first-principles calculations of the lattice properties of cubic diamond, hexagonal diamond, cubic boron nitride, and wurtzite boron nitride. We found that the cubic phases have a much higher lattice thermal conductivity than the hexagonal phases at room temperature, despite of their similar bonding environments. By analyzing phonon properties, we revealed that hexagonal phases have significantly higher phonon

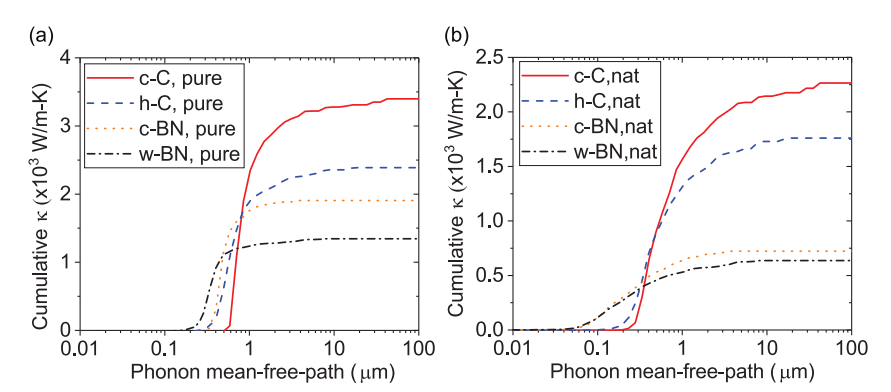


Fig. 7. Cumulative thermal conductivity with respective to the phonon mean-free-path for c-C, h-C, c-BN, and w-BN at 300 K and 0 Pa for (a) isotopically pure materials and (b) materials containing isotopes with natural abundance. (A colour version of this figure can be viewed online.)

scattering rates than their corresponding cubic phases. This is caused by the enlarged phonon scattering phase space in hexagonal phases, which arises from the increased number of optical phonon modes in hexagonal structures. We also explored the effect of high pressure on thermal transport in those four materials and found that a high pressure of 125 GPa, which is typical in applications of superhard materials, can lead to a two-to three-fold increase in  $\kappa_L$  at room temperature in isotopically pure samples. This is caused by the combined effect of increased phonon group velocity (minor) and reduced phonon scattering rates (major). In particular, the reduction in the phonon scattering rates under high pressure is attributed to the shrinked volume of 3-phonon scattering phase space, which is caused by the enlarged optical-acoustic phonon bandgap. This work revealed the significant role of lattice structure in determining the lattice thermal transport properties of materials. It also uncovered the prominent effect of high pressure on the  $\kappa_L$  of diamonds and boron nitrides, which is crucial for the application of these superhard materials.

## Acknowledgment

P.C., G.X., and Y.W. would like to thank the faculty startup fund from the University of Nevada, Reno. P.C. and L.C. are also grateful to the financial support from the National Science Foundation (Grant No. CMMI-1727428) and the faculty startup fund from the University of Nevada, Reno.

## Appendix A. Supplementary data

Supplementary data related to this article can be found at https://doi.org/10.1016/j.carbon.2018.06.025.

#### References

- R. Berman, P.R.W. Hudson, M. Martinez, Nitrogen in diamond: evidence from thermal conductivity, J. Phys. C Solid State Phys. 8 (21) (1975) L430. http:// stacks.iop.org/0022-3719/8/i=21/a=003.
- [2] E. Burgemeister, Thermal conductivity of natural diamond between 320 and 450 k, Phys. B+C 93 (2) (1978) 165–179. https://doi.org/10.1016/0378-4363(78)90123-7. http://www.sciencedirect.com/science/article/pii/0378436378901237.
- [3] L. Wei, P.K. Kuo, R.L. Thomas, T.R. Anthony, W.F. Banholzer, Thermal conductivity of isotopically modified single crystal diamond, Phys. Rev. Lett. 70 (1993) 3764–3767, https://doi.org/10.1103/PhysRevLett.70.3764. https://link.aps.org/doi/10.1103/PhysRevLett.70.3764.
- [4] D.A. Broido, L. Lindsay, A. Ward, Thermal conductivity of diamond under extreme pressure: a first-principles study, Phys. Rev. B 86 (2012), 115203, https://doi.org/10.1103/PhysRevB.86.115203. https://link.aps.org/doi/10. 1103/PhysRevB.86.115203.
- [5] A.A. Balandin, Thermal properties of graphene and nanostructured carbon materials, Nat. Mater. 10 (8) (2011) 569.
- [6] L. Lindsay, D.A. Broido, N. Mingo, Flexural phonons and thermal transport in

- graphene, Phys. Rev. B 82 (2010), 115427, https://doi.org/10.1103/Phys-RevB.82.115427. https://link.aps.org/doi/10.1103/PhysRevB.82.115427.
- [7] Y. Wang, A.K. Vallabhaneni, B. Qiu, X. Ruan, Two-dimensional thermal transport in graphene: a review of numerical modeling studies, Nanoscale Microscale Thermophys. Eng. 18 (2) (2014) 155–182.
- [8] Y. Wang, A. Vallabhaneni, J. Hu, B. Qiu, Y.P. Chen, X. Ruan, Phonon lateral confinement enables thermal rectification in asymmetric single-material nanostructures, Nano Lett. 14 (2) (2014) 592–596, https://doi.org/10.1021/ nl403773f pMID: 24393070, https://doi.org/10.1021/nl403773f, https://doi. org/10.1021/nl403773f.
- [9] E.K. Sichel, R.E. Miller, M.S. Abrahams, C.J. Buiocchi, Heat capacity and thermal conductivity of hexagonal pyrolytic boron nitride, Phys. Rev. B 13 (1976) 4607–4611, https://doi.org/10.1103/PhysRevB.13.4607. https://link.aps.org/ doi/10.1103/PhysRevB.13.4607.
- [10] I. Jo, M.T. Pettes, J. Kim, K. Watanabe, T. Taniguchi, Z. Yao, L. Shi, Thermal conductivity and phonon transport in suspended few-layer hexagonal boron nitride, Nano Lett. 13 (2) (2013) 550–554, https://doi.org/10.1021/nl304060g pMID: 23346863, https://doi.org/10.1021/nl304060g, https://doi.org/10.1021/ nl304060g.
- [11] H. Zhou, J. Zhu, Z. Liu, Z. Yan, X. Fan, J. Lin, G. Wang, Q. Yan, T. Yu, P.M. Ajayan, J.M. Tour, High thermal conductivity of suspended few-layer hexagonal boron nitride sheets, Nano Res. 7 (8) (2014) 1232–1240, https://doi.org/10.1007/s12274-014-0486-z. https://doi.org/10.1007/s12274-014-0486-z.
- [12] N. V. Novikov, T. D. Osetinskaya, A. A. Shul'zhenko, A. P. Podoba, A. N. Sokolov, I. A. Petrusha, Akad. Nauk Ukr. RSR, Ser. A: Fiz.-Tekh. Mat. Nauki 72.
- [13] L. Lindsay, D.A. Broido, T.L. Reinecke, First-principles determination of ultrahigh thermal conductivity of boron arsenide: a competitor for diamond? Phys. Rev. Lett. 111 (2013), 025901 https://doi.org/10.1103/Phys-RevLett.111.025901. https://link.aps.org/doi/10.1103/PhysRevLett.111. 025901.
- [14] Z. Pan, H. Sun, Y. Zhang, C. Chen, Harder than diamond: superior indentation strength of wurtzite bn and lonsdaleite, Phys. Rev. Lett. 102 (2009), 055503, https://doi.org/10.1103/PhysRevLett.102.055503. https://link.aps.org/doi/10. 1103/PhysRevLett.102.055503.
- [15] M. Omini, A. Sparavigna, Beyond the isotropic-model approximation in the theory of thermal conductivity, Phys. Rev. B 53 (1996) 9064–9073, https:// doi.org/10.1103/PhysRevB.53.9064. https://link.aps.org/doi/10.1103/ PhysRevB.53.9064.
- [16] M. Omini, A. Sparavigna, Heat transport in dielectric solids with diamond structure, Nuovo Cimento-Soc. Itali. Fisi. Sezione D 19 (1997) 1537–1564.
- [17] A. Sparavigna, Influence of isotope scattering on the thermal conductivity of diamond, Phys. Rev. B 65 (2002), 064305, https://doi.org/10.1103/Phys-RevB.65.064305. https://link.aps.org/doi/10.1103/PhysRevB.65.064305.
- [18] D.A. Broido, M. Malorny, G. Birner, N. Mingo, D.A. Stewart, Intrinsic lattice thermal conductivity of semiconductors from first principles, Appl. Phys. Lett. 91 (23) (2007), 231922, https://doi.org/10.1063/1.2822891. https://doi.org/10. 1063/1.2822891. https://doi.org/10.1063/1.2822891.
- [19] W. Li, J. Carrete, N.A. Katcho, N. Mingo, Shengbte: a solver of the Boltzmann transport equation for phonons, Comput. Phys. Commun. 185 (6) (2014) 1747–1758. https://doi.org/10.1016/j.cpc.2014.02.015. http://www.sciencedirect.com/science/article/pii/S0010465514000484.
- [20] J.M. Ziman, Electrons and Phonons: the Theory of Transport Phenomena in Solids, Oxford University Press, 1960.
- [21] A. Ward, D. Broido, D.A. Stewart, G. Deinzer, Ab initio theory of the lattice thermal conductivity in diamond, Phys. Rev. B 80 (12) (2009), 125203.
  [22] A.J. Ladd, B. Moran, W.G. Hoover, Lattice thermal conductivity: a comparison
- 22] A.J. Ladd, B. Moran, W.G. Hoover, Lattice thermal conductivity: a comparison of molecular dynamics and anharmonic lattice dynamics, Phys. Rev. B 34 (8) (1986), 5058.
- [23] G. Deinzer, G. Birner, D. Strauch, Ab initio calculation of the linewidth of various phonon modes in germanium and silicon, Phys. Rev. B 67 (14) (2003), 144304.
- [24] Y. Wang, Z. Lu, X. Ruan, First principles calculation of lattice thermal

- conductivity of metals considering phonon-phonon and phonon-electron scattering, J. Appl. Phys. 119 (22) (2016), 225109, https://doi.org/10.1063/1.4953366. https://doi.org/10.1063/1.4953366. https://doi.org/10.1063/1.4953366.
- [25] P. Giannozzi, S. Baroni, N. Bonini, M. Calandra, R. Car, C. Cavazzoni, D. Ceresoli, G.L. Chiarotti, M. Cococcioni, I. Dabo, A.D. Corso, S. de Gironcoli, S. Fabris, G. Fratesi, R. Gebauer, U. Gerstmann, C. Gougoussis, A. Kokalj, M. Lazzeri, L. Martin-Samos, N. Marzari, F. Mauri, R. Mazzarello, S. Paolini, A. Pasquarello, L. Paulatto, C. Sbraccia, S. Scandolo, G. Sclauzero, A.P. Seitsonen, A. Smogunov, P. Umari, R.M. Wentzcovitch, Quantum espresso: a modular and open-source software project for quantum simulations of materials, J. Phys. Condens. Matter 21 (39) (2009) 395502. http://stacks.iop.org/0953-8984/21/i=39/a=395502.
- [26] P. Giannozzi, O. Andreussi, T. Brumme, O. Bunau, M.B. Nardelli, M. Calandra, R. Car, C. Cavazzoni, D. Ceresoli, M. Cococcioni, N. Colonna, I. Carnimeo, A.D. Corso, S. de Gironcoli, P. Delugas, R.A.D. Jr, A. Ferretti, A. Floris, G. Fratesi, G. Fugallo, R. Gebauer, U. Gerstmann, F. Giustino, T. Gorni, J. Jia, M. Kawamura, H.-Y. Ko, A. Kokalj, E. Kkbenli, M. Lazzeri, M. Marsili, N. Marzari, F. Mauri, N.L. Nguyen, H.-V. Nguyen, A.O. de-la Roza, L. Paulatto, S. Poncā, D. Rocca, R. Sabatini, B. Santra, M. Schlipf, A.P. Seitsonen, A. Smogunov, I. Timrov, T. Thonhauser, P. Umari, N. Vast, X. Wu, S. Baroni, Advanced capabilities for materials modelling with q uantum espresso, J. Phys. Condens. Matter 29 (46) (2017) 465901. http://stacks.iop.org/0953-8984/29/i=46/a=465901.
- [27] Supplementary materials.
- [28] N. Troullier, J.L. Martins, Efficient pseudopotentials for plane-wave calculations, Phys. Rev. B 43 (1991) 1993–2006, https://doi.org/10.1103/Phys-RevB.43.1993. http://link.aps.org/doi/10.1103/PhysRevB.43.1993.
- [29] D.G. Onn, A. Witek, Y.Z. Qiu, T.R. Anthony, W.F. Banholzer, Some aspects of the thermal conductivity of isotopically enriched diamond single crystals, Phys. Rev. Lett. 68 (1992) 2806–2809, https://doi.org/10.1103/PhysRevLett.68.2806. https://link.aps.org/doi/10.1103/PhysRevLett.68.2806.
- [30] D. Tabor, The hardness of solids, Rev. Phys. Technol. 1 (3) (1970) 145.
- [31] B. Wu, J.-a. Xu, Total energy calculations of the lattice properties of cubic and hexagonal diamond, Phys. Rev. B 57 (21) (1998), 13355.
- [32] H. Holloway, K. Hass, M. Tamor, T. Anthony, W. Banholzer, Isotopic dependence of the lattice constant of diamond, Phys. Rev. B 44 (13) (1991) 7123.
   [33] F.P. Bundy, I.S. Kasper, Hexagonal diamonda new form of carbon, I. Chem.
- [33] F.P. Bundy, J.S. Kasper, Hexagonal diamonda new form of carbon, J. Chem. Phys. 46 (9) (1967) 3437–3446, https://doi.org/10.1063/1.1841236. https://doi.org/10.1063/1.1841236.
- [34] S.R.P. Silva, G.A.J. Amaratunga, E.K.H. Salje, K.M. Knowles, Evidence of hexagonal diamond in plasma-deposited carbon films, J. Mater. Sci. 29 (19) (1994) 4962–4966, https://doi.org/10.1007/BF01151085. https://doi.org/10.1007/BF01151085.
- [35] E. Knittle, R.M. Wentzcovitch, R. Jeanloz, M.L. Cohen, Experimental and theoretical equation of state of cubic boron nitride, Nature 337 (6205) (1989) 349.
- [36] A. Nagakubo, H. Ogi, H. Sumiya, K. Kusakabe, M. Hirao, Elastic constants of

- cubic and wurtzite boron nitrides, Appl. Phys. Lett. 102 (24) (2013), 241909, https://doi.org/10.1063/1.4811789. https://doi.org/10.1063/1.4811789. https://doi.org/10.1063/1.4811789.
- [37] R.H.W. Jr, Cubic form of boron nitride, J. Chem. Phys. 26 (4) (1957), https://doi.org/10.1063/1.1745964, 956-956, https://doi.org/10.1063/1.1745964, https://doi.org/10.1063/1.1745964.
- [38] J. Tersoff, Modeling solid-state chemistry: interatomic potentials for multi-component systems, Phys. Rev. B 39 (1989) 5566–5568, https://doi.org/10.1103/PhysRevB.39.5566. https://link.aps.org/doi/10.1103/PhysRevB.39.5566
- [39] J. Tersoff, Erratum: modeling solid-state chemistry: interatomic potentials for multicomponent systems, Phys. Rev. B 41 (1990), https://doi.org/10.1103/ PhysRevB.41.3248.2, 3248—3248, https://link.aps.org/doi/10.1103/PhysRevB. 41.3248.2.
- [40] M.S. Green, Markoff random processes and the statistical mechanics of timedependent phenomena. ii. irreversible processes in fluids, J. Chem. Phys. 22 (3) (1954) 398–413, https://doi.org/10.1063/1.1740082. https://doi.org/10. 1063/1.1740082. https://doi.org/10.1063/1.1740082.
- [41] R. Kubo, M. Yokota, S. Nakajima, Statistical-mechanical theory of irreversible processes. ii. response to thermal disturbance, J. Phys. Soc. Jpn. 12 (11) (1957) 1203–1211, https://doi.org/10.1143/JPSJ.12.1203. https://doi.org/10.1143/ JPSJ.12.1203. https://doi.org/10.1143/JPSJ.12.1203.
- [42] R. Vogelsang, C. Hoheisel, G. Ciccotti, Thermal conductivity of the lennard-jones liquid by molecular dynamics calculations, J. Chem. Phys. 86 (11) (1987) 6371–6375, https://doi.org/10.1063/1.452424. https://doi.org/10.1063/1.452424. https://doi.org/10.1063/1.452424.
- [43] S. Plimpton, Fast parallel algorithms for short-range molecular dynamics, J. Comput. Phys. 117 (1) (1995) 1–19. https://doi.org/10.1006/jcph.1995.1039. http://www.sciencedirect.com/science/article/pii/S002199918571039X.
- [44] Z. Fan, L.F.C. Pereira, H.-Q. Wang, J.-C. Zheng, D. Donadio, A. Harju, Force and heat current formulas for many-body potentials in molecular dynamics simulations with applications to thermal conductivity calculations, Phys. Rev. B 92 (2015), 094301, https://doi.org/10.1103/PhysRevB.92.094301. https://link. aps.org/doi/10.1103/PhysRevB.92.094301.
- [45] S.-i. Tamura, Y. Tanaka, H.J. Maris, Phonon group velocity and thermal conduction in superlattices, Phys. Rev. B 60 (1999) 2627–2630, https://doi.org/10.1103/PhysRevB.60.2627. https://link.aps.org/doi/10.1103/PhysRevB.60.
- [46] E.S. Landry, A.J.H. McGaughey, Effect of film thickness on the thermal resistance of confined semiconductor thin films, J. Appl. Phys. 107 (1) (2010), 013521, https://doi.org/10.1063/1.3275506. https://doi.org/10.1063/1.3275506.
- [47] Y. Wang, H. Huang, X. Ruan, Decomposition of coherent and incoherent phonon conduction in superlattices and random multilayers, Phys. Rev. B 90 (2014), 165406, https://doi.org/10.1103/PhysRevB.90.165406. https://link.aps. org/doi/10.1103/PhysRevB.90.165406.